Available online at www.sciencedirect.com

ScienceDirect

Procedia Manufacturing 47 (2020) 1190–1196

Procedia MANUFACTURING

www.elsevier.com/locate/procedia

23rd International Conference on Material Forming (ESAFORM 2020)

A Simple Approach to Stiffness Enhancement of a Printable Shape by Hamilton-Jacobi Skeletonization

Michael Breuß[a,*], Johannes Buhl[c], Ashkan Mansouri Yarahmadi[a], Markus Bambach[c], Pascal Peter[b]

[a]*BTU Cottbus-Senftenberg, Applied Mathematics Group, Platz der Deutschen Einheit 1, 03046 Cottbus, Germany*
[b]*Saarland University, Mathematical Image Analysis Group, Campus E1.7, 66041 Saarbrücken, Germany*
[c]*Chair of Mechanical Design and Manufacturing (KuF), Brandenburg University of Technology Cottbus-Senftenberg, Konrad-Wachsmann-Allee 17, 03046 Cottbus, Germany*

* Corresponding author. Tel.: +49-355-692086 ; fax: +49-355-692402. *E-mail address:* breuss@b-tu.de

Abstract

The 3D-Printing technology is ready to produce parts with specific properties like individual stiffness. Based on a predefined outer shape, the inner structure of a printed part defines mainly the mechanical features. By Hamilton-Jacobi skeletonization, a stiffness enhancement of a printable shape can be achieved in a way, that a novel AM-corner includes linear axis function. Originating in the field of shape analysis in computer vision and graphics, the so-called medial axis transform (MAT) is designed for the computation of a structure that resembles the bone structure of biological shapes. The input for MAT computation is typically a shape's boundary. The arising topological skeletons have proven to provide a useful concept for many applications; however, their computation is generally intricate and also known to rely on many parameters, diminishing the accessibility of skeletonization methods. In this work, the classical Hamilton-Jacobi skeletonization approach is adopted to compute a stability enhancing shape structure. As the basic method has not been designed for the context of additive manufacturing, a set of suitable modifications are introduced to design an algorithm that suits our intended purpose. Unlike the traditional skeletonization schemes, the resulting method appears to be robust and in practice almost completely automated as we can identify useful generic parameter settings. By a finite element method (FEM) study, the elastic stress properties of the AM-corner with linear axis function is validated and printed with in metal (1.4404) with the 3D Selected Laser Melting (SLM) system AconityMIDI. The AM-knot with skeletonization guides approximately 20 times better than a standard knot. While the first obtained results are shown as 2.5 dimensional shapes, it is emphasized that the proposed algorithm offers many possibilities for extensions to three dimensions and variations in context of additive manufacturing.

Keywords: Skeletonization; Hamilton-Jacobi skeletonization; stiffness enhancement; 3D printing; additive manufacturing

1. Introduction

In additive manufacturing (AM), the problem arises how to find an inner structure of a shape represented by its other geometry (boundary), which may enhance the shapes' mechanical properties, for example, the stiffness at a reasonable added material. With the rapid progress and availability of 3D printing technology, it would also be desirable to make a corresponding procedure fast and largely automated, so that any user could employ it easily as a tool but still has some design choices left. Many computational methods have been developed to fix digital models proposed by a user so as to make them stiffer, based for example on structural analysis [1,2], balance analysis of static and rotational objects [3,4], or deformation behavior [5]. However, all these methods have in common that they are computationally complex and not easy to use. On the other hand, it appears to be a natural idea to construct a kind of skeleton-like supportive structure of a given shape, under the condition that it has to be connected in a reasonable way to the shape boundary.

Interestingly, the classic medical axis transform (MAT) from computer vision and graphics offers a means to compute structures that at first glance resemble biological skeletons, and thus the MAT is also called skeletonization. Initially, the MAT was introduced in 1967 by Blum [6] as a mathematical tool for

10.1016/j.promfg.2020.04.147

modelling the biological problem of shape vision. The standard skeleton from computer vision represents a shape by a thin set of lines or arcs that are centered in the shape, eliminating superfluous information of local symmetries. Due to its useful properties, including equivalence to the shape boundary, homotopy to the original shape (meaning the skeleton can be transformed into the original shape) and invariance under Euclidean transformations, the MAT has been used for numerous practical applications, see e.g. [7,8] for an overview. However, while the principle usefulness of the MAT is undeniable, the corresponding algorithms are often complex and lack accessibility because they depend on many parameters. Also the robustness of an implementation of the MAT approach is an important issue.

In spite of the latter aspects, skeletonization methods have already been adopted for certain uses in 3D printing. In [9], a standard skeletonization scheme has been employed to set up a fast computational model for structural analysis of shapes. Note that, the standard computer vision skeletons are not connected systematically to the shape boundaries. This connection issue is fixed in [9] by employing in a separate step, a skin binding technique provided by computer graphics software. Furthermore, skeletonization is not used in [9] as a tool for computing supportive structures. In [10,11], the authors make beneficial use of the geometric properties of the MAT to compute contour-based path patterns which offset parallel to the boundary of the object's geometry. The construction using parallel contours is desirable for printing thin metallic structures in wire and arc additive manufacturing. Both of the latter works [10,11] focus solely on corresponding path planning for printing.

Turning to the contributions of this paper, the framework of Hamilton-Jacobi skeletonization introduced in [12], and more specifically one of its extensions presented in [13], is adapted to compute a stability enhancing structure for a given shape. Here, the basic approach is modified to obtain skeletons which are (i) connected to the shape boundary to support it, (ii) thick enough to be printable as a supportive structure, and (iii) defined in a recursive way which may allow to adapt to complex geometries. Thereby, the depth of the recursion can be defined by the user.

The proposed approach to skeletonization automatically introduces additional structures that are perpendicular to the shape boundary, and results in an end-to-end internal connected structure. In addition, the recursive property offers a way to support the additional structures. The resulting method is in practice free of other parameters than the depth of the recursion, resulting in a setting that can be employed robustly in a one-size-fits-all manner. As presented here, the proposed novel method concentrates on 2.5-dimensional shapes, yet by the techniques employed for its construction one may note already here that the skeletonization method is conceptually extendable to three dimensions.

2. Computation of Stability Enhancing Structures by Hamilton-Jacobi Skeletonization

The purpose of this section is to briefly recall relevant parts of the flux-ordered thinning (FOT) approach as presented in [13] rooted by the modeling on Hamiltonian physics, and discuss the new adaptations to it. As the main motivation to make use of the approach provided in [13], one can mention its potential to robustly estimate the physically justified shock locations – identical to skeleton locations – in the underlying eikonal equation, as described in some more detail below.

2.1. Algorithmic set-up

In this paragraph, the underlying set-up of the algorithm is illuminated. It operates on a binary image $u: \Omega \subset R^2 \mapsto \{0,1\}$ that represents the shapes' domain as well as some background information. In the image domain Ω one may especially consider the object domain O over which the shape is printed and its boundary ∂O.

Of particular importance is the Euclidean distance map D of the object boundary. The distance map is defined for any point in O by its closest distance to a boundary point. As one has to work with points on a discrete two-dimensional grid, for simplicity a uniform spatial mesh width of one in both directions is considered here. For the computation of the distance map, the boundary points are set to the zero and the distance values' computation is performed by the algorithm [14]. The latter method, is a sequential algorithm computing the distance map of a binary image in O(N), with N to be the total number of pixels. In [14], the Euclidean distance map is computed based on a Voroni-feature map obtained from the binary image. One may note, that there are many suitable ways to obtain a binary image distance map, see e.g. the discussion in [13].

It is surely adequate to explain, that the contour lines of the distance map are running parallel to the shape boundary. The basic idea of the MAT aims at identifying those points where the contour lines become one dimensional, i.e. where there is a significant part of the boundary at an equal distance from such a point (See Fig. 1).

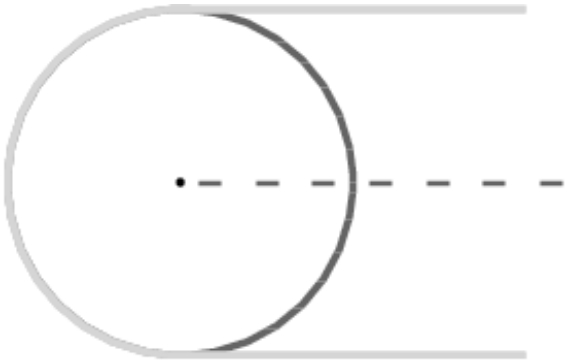

Fig. 1. A one-dimensional contour, shown as dashed line, that is equidistant from the shape boundary. The shape boundary is shown as light gray that partially overlaps with a circle visualized in dark gray. The most left point of the skeleton is equidistant from the circle part of the boundary and the rest part of the skeleton has the same distance from the horizontal sections of the boundary. Note, the skeleton is continuous, and is shown here as dashed lines only for the purpose of visualization.

In Fig. 2, the corresponding distance map is given with respect to the shape boundary shown in Fig. 1. The nested

contour lines are parallel to the shape boundary. Because the gradient vectors, shown as red arrows in Fig. 2, are perpendicular to the contour lines and pointing to the inside of the shape, one may thus find useful candidates for skeleton points by considering the sinks of the gradient vector field ∇D.

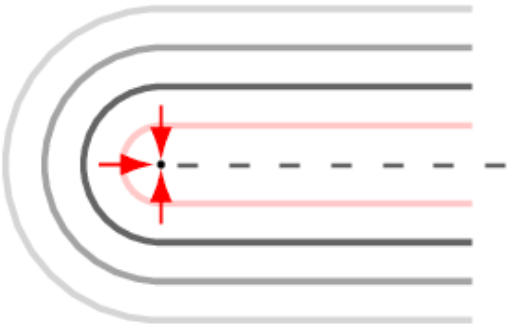

Fig. 2. A set of contour lines corresponding to a distance map. They belong to a shape whose boundary is shown as the most outer contour. As one observes, the contours are established parallel to the shape boundary. A set of points, shown as dashed lines, represent the skeleton of the shape and are equidistant from the shape boundary. The red arrows represent the gradient vectors corresponding to a particular skeleton point that is considered as a sink point of the gradient vector field corresponding to the distance map.

Given the computed distance map, one can make use of the values of its gradient. To this end, the components of the gradient vector are evaluated pointwise by making use of a finite difference discretization of the corresponding derivatives. In this work the standard Sobel operator often used in image processing is employed, which is a weighted average of central differences. In x-direction, the Sobel operator reads as

$$\begin{bmatrix} -1 & 0 & +1 \\ -2 & 0 & +2 \\ -1 & 0 & +1 \end{bmatrix}. \tag{1}$$

The shown operator in (1) is evaluated over Ω using zero-valued Dirichlet boundary conditions.

Coming back to the mentioned idea concerned with the use of ∇D, one may stress that this is at the heart of the Hamilton-Jacobi skeletonization [12] and for the flux-order thinning strategy introduced for the first time there. The sinks can be identified by taking the divergence of the gradient vector field. To compute the quantity $\mathrm{div}\nabla D$ efficiently on the discrete grid, as in [13] the average outward flux for each point $\mathrm{p} \in \Omega$ obtained as

$$F(p) = \frac{1}{8}\sum_{i=1}^{8} \nabla D\big(n_i(p)\big) \cdot N\big(n_i(p)\big) \tag{2}$$

is employed in this paper. Thereby $n_1(p), \dots n_8(p)$ are the eight direct neighbors of p on the discrete image grid, and $N\big(n_i(p)\big)$ denotes the outward normal pointing from p to $n_i(p)$.

The resulting flux map F is used to define the thinning order, i.e. the order by which points are successively removed from a given object until the desired skeleton structure remains. In the thinning step of the procedure, the high-order flux values are removed first from the corresponding priority queue until a certain threshold value τ is reached. As also for instance in [12,13] a homotopic thinning [15] is used here in addition, meaning that thinning candidates are only removed if the resulting structure has the same number and configuration of connected components and holes as the original shape.

2.2. Discussion

In typical image-processing applications, it is desirable that the resulting skeleton is relatively thin, meaning that the threshold τ is chosen in a way that the skeleton is usually not connected to the boundary and has a width of about one pixel, see Fig. 3. In contrast, here a relatively high threshold is employed in order to connect the computed structure to the shape boundary.

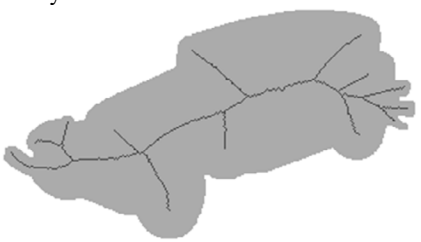

Fig. 3. A typical skeleton in context of image processing as obtained in [13]. The skeleton has one-pixel width, it is fully connected and not in touch with the boundary of the car object.

One may comment at this point also on some important observations. Due to the underlying construction making use of the distance field, the results obtained in the described way are quite robust versus small distortions of the boundary which may be a typical problem with many skeletonization algorithms. The arising robustness may be related to the fact that one may compute the distance field via the eikonal equation. This problem may be cast as a standard boundary value problem for the latter partial differential equation which is supposed to be well-posed in a setting such as the one in this paper. Secondly, since the aim of the method is not to compute extremely thin skeleton structures, it does not suffer from the phenomenon that whole branches of the skeleton are lost in case the threshold effectively makes such a distinction. This high dependence on the threshold in the definition of thin branches is one of the standard problems of the basic approach in classic applications. Related to the latter aspect the issue is that one also does not run here into the problem to obtain many unconnected thin candidate structures that are either semantically important or should be pruned, which is again a point where automatically by construction and in the particular application tackled in this paper a difficult aspect of classic skeletonization is avoided.

Summarizing these observations, for the application in this work the choice of the underlying skeletonization method makes an important difference among the many possible approaches to skeletonization cf. [7,13]. The method of choice presented here combines some beneficial aspects with a simple, global choice of the threshold parameter, which makes it simple and robust.

2.3. Adaptations and test case

While the parameter τ is in this paper chosen manually, it is possible to compute automatically a robust estimate for it given a typical size of an input image (respectively depicted objects), see [13]. In experiments not report here in detail, skeletonization results are very robust in the regime of high threshold values as predicted by the discussion in Paragraph 2.2.

The aim is now to discuss some adaptations of the existing skeletonization method, see Figs. 5 and 6 for illustrations. As shown in Fig. 4 the computed skeleton is to be added to the boundary points of a given shape. One may introduce for instance thickening of appearing structures e.g. by morphological filtering in the digital domain, see also comments on morphological filtering below. In addition, as one observes in Fig. 5, it is proposed here that the final structure may be enhanced by a recursive application of the skeletonization approach. This is surely an algorithmic novelty in this context. Moreover, as one has to thicken the connections between skeleton points as well as its connections to the shape boundary in low resolution shapes, here a generic post-processing step in terms of a morphological dilation operation using a 2×2 structuring element is employed, compare e.g. [16]. This effectively means that all computed structures are thicken by point in any direction.

The proceeding is illustrated with an experiment based on the symmetric shape shown in Fig. 6a, in white color against its background. As explained a printable support structure visualized in Fig. 6b is obtained corresponding to the shape shown in Fig. 6a. The printable structure is the result of merging the initial boundary and the skeleton of its corresponding shape. The same printable structure as shown in Fig. 6b is once again shown as Fig. 7 in a bigger scale so that its details can be clearly observed.

In the next section, the stiffness behavior of the printable structure shown in Fig. 8 is investigated.

3. Novel AM-knots including Linear Axis Function

In printers, cars or in general in mechanical engineering, elastic deformable components are required, which feature movements with a stiffness similar to a linear axis with a specific spring stiffness and are designed as fixed in all other directions (see Fig. 8).

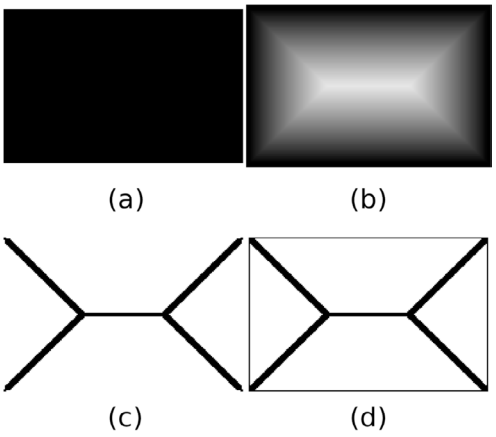

Fig. 4. (a) A shape of interest, namely a black rectangle; and (b) its computed distance map with lighter values to represent those pixels with the farthest distances to the boundary (c) the skeleton corresponding to the shape of interest obtained by adopting the approach [13]; and finally (d) the printable support structure obtained by merging the skeleton shown in (c) and the boundary of the initial shape.

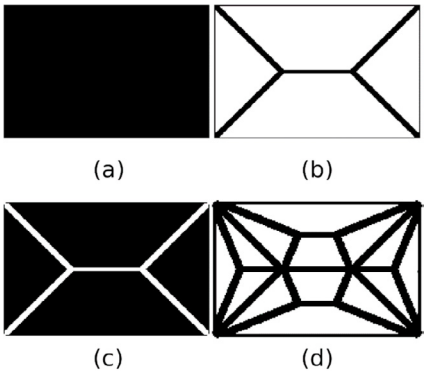

Fig. 5. (a) The initial black rectangular shape; and (b) its obtained skeleton; (c) the modified black rectangle while its skeleton being subtracted from it; (d) the final printable support structure obtained by assimilating the skeleton shown in (b), the skeleton corresponding to the modified rectangle and the boundary of the initial black rectangle.

With high-precision metal 3D printing, it is possible to equip connecting nodes directly with such a guiding and spring function. Fig. 9 shows knots with a stiffness individual adjusted by the rib structure. The bearing of this knot with linear axis function is encased with rips, which transmits the load to the two outer and the middle rip. The idea behind the linear axis function is, that the main rips have the capability to

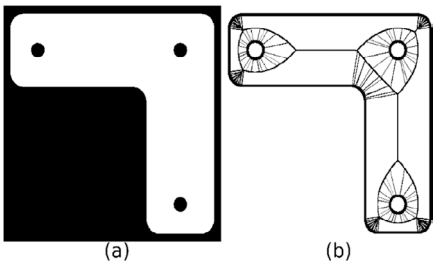

Fig. 6. (a) A shape of interest shown on black background; (b) Its corresponding printable structure obtained based on [13].

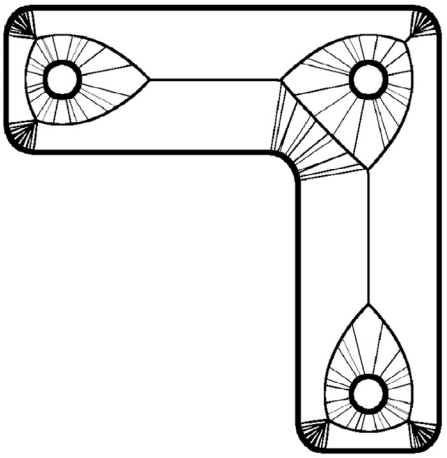

Fig. 7. The same printable structure as shown in Fig. 6 but in higher resolution. The structure is merged from the skeleton obtained based on [13] and the boundary of the shape.

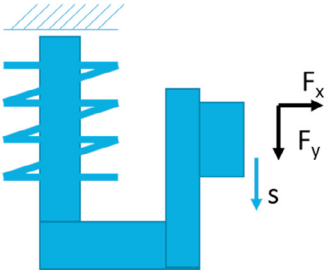

Fig. 8. The principle sketch of a guide with individual stiffness behavior.

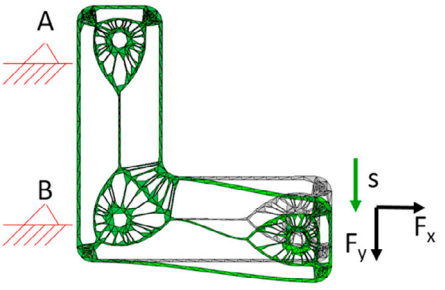

Fig. 9. The Novel AM-corners including linear axis function.

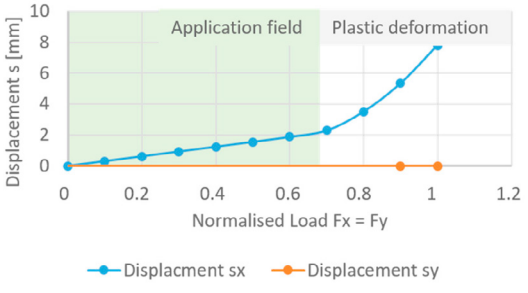

Fig. 10. The principle sketch of a guide with individual stiffness behavior.

deform elastically and are able to move the free junction parallel to the y-axis. Another feature of the AM-knot should be the possibility to shift the working area, in which the linear axis function is stable. This condition can be achieved with overloading the knot. The knot spring back into a stable pre-stressed position. Pre-stressed knots should feature an accelerate stiffness.

3.1. FEM-Simulation of the AM-knots with individual stiffness

To evaluate the stiffness of the rib structure, a mechanical model with FEM is established in Abaqus. In this work, the manufacturing process is not considered in detail, which introduces local properties and residual stresses [17]. The metal 1.4404 is described with a Young´s modulus of E = 200.000 N/mm², a Poisson´s ratio of 0.3 and a density of 7.874 g/cm³. To achieve different working areas of the knot, the flow behavior of the metal begins with the yield strength of R_{eH} = 400N/mm² and follows an isotropic hardening law.

The geometry of the knot is modeled with a quadratic meshed shell with 5-integration points over the thickness of 10mm. The outer dimensions of the AM-knot are 100 mm × 100 mm width and length. The outer skeleton of the structure has a width of 1.3mm and the inner rips differ. The calculation itself is done with the direct implicit solver. Therefore, the full Newton is used without automatic stabilization. Both bearing A and B are modelled with boundary conditions, which allows rotation and inhibit displacement.

For a normalized force of $F_x = F_y$, an approximately parallel displacement of the load application point can be seen (Table 1).

Table 1. Load cases I-III with the plastic deformation as result

Load Case	Load Fx [N]	Load Fy [N]	Plastic Strain
I	50	50	0
II	100	100	0
III	200	200	0.02

The knot can be loaded with 100N in x and y direction without plastic deformation. As shown in Fig. 10 the stiffness rises linear with displacement. The guiding function can be used directly after printing, because typical phenomenon of springs, like changing surface stiffness's, are prevented.

If the knot is overloaded (200 N), plastic deformation occurs in the rib structure, which leads to a change in the spring stiffness (see Fig. 10). At the maximum displacement in the application field, the linear axis shows a shift in the working direction of s_x = 2.2 mm and in guiding direction and in perpendicular direction s_y = 0.0009 mm. As already mentioned, a plastic deformed knot features an application field with a higher stiffness. This condition can be achieved with an overload, whereby the initial position will change too. In Fig. 11 the von Mises Stress is shown during plastic deformation at a force of $F_x = F_y$ =200 N and in Fig. 12 the geometry with the position after spring back can be seen.

3.2. Comparison with a standard profile

To evaluate the rip structure, the outer profile is taken and a thick rip is constructed in the middle of the profile. Some more rips are designed in the corners of the profile. The calculation with the same material properties shows, that the stress in a standard knot is lower (see. Fig. 13 for $F_x = F_y = 200$ N), which means, that the working area decreases for the AM-knot. However, the displacement of the standard knot in y-direction is $s_y = 0.023$ mm ($F_x = F_y = 50$ N). This means, that the Novel AM- knot features approximately 20 times more accurate than a standard knot, which seems to be highly useful.

3.3. AM of the knots including Linear Axis Function

The knot was printed with the 3D Selected Laser Melting (SLM) system AconityMIDI. The printer uses powder (1.4404) which is heated layer by layer locally with the laser. Because the powder is heated above the melting temperature and argon atmosphere is used to prevent oxidation during the process. The used laser power was 245 W at a scanning speed of 1500 mm/s. To save production time the geometry has been scaled with a factor of 0.5.

The printed knot can be seen in top and perspective views as Figs. 14 and 15 directly after printing. As displayed in the perspective view, the support structure connects the knot with the base plate of the printer and must be removed in a finishing process before the assembly process.

4. Conclusion and Outlook

A working method that gives a simple and effective procedure for introducing additional structures that enhance the stiffness of a given shape is presented here. The underlying method has its mathematical root in Hamiltonian physics. Thus, it has a highly flexible modelling background based on which one could explore properties of materials and the printing process itself. The method is in practice parameter-free which facilitates simple use of it. The presentation focused on 2.5 dimensions, however all crucial components like distance and flux map computation are readily extendable to the full 3D setting, a setting that will be explored in the future.

The most intricate part in the extension of the underlying skeletonization method is surely the homotopic thinning process which could be further adapted to applications in additive manufacturing.

It should be noted that a possible extension to three dimensions of skeletonization structures as constructed here gives by design bone-like and elongated, which may facilitate the printing process for instance in getting out powder originating from the printing system. However, based on related algorithms this may be modified and other structures could be introduced. One may also conjecture that the recursive approach introduced in this paper could be even more beneficial in the 3D setting. Furthermore, as shown in other works mentioned in the introduction, one could make broader use of the underlying computations, e.g. by combining skeleton construction and path planning.

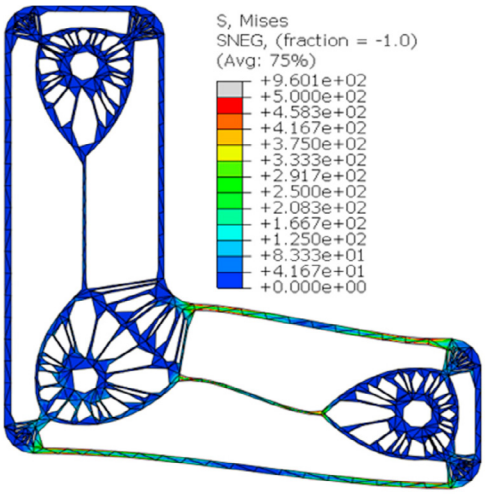

Fig. 11. Von Mises Stress during plastic deformation at a force of $F_x = F_y = 200$N

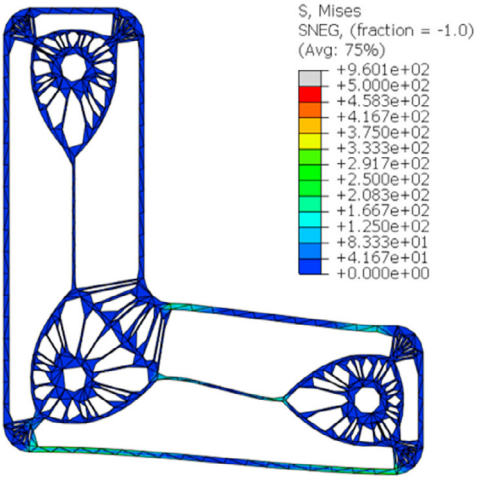

Fig. 12. Von Mises Stress during plastic deformation at a force of $F_x = F_y = 200$N, after spring back

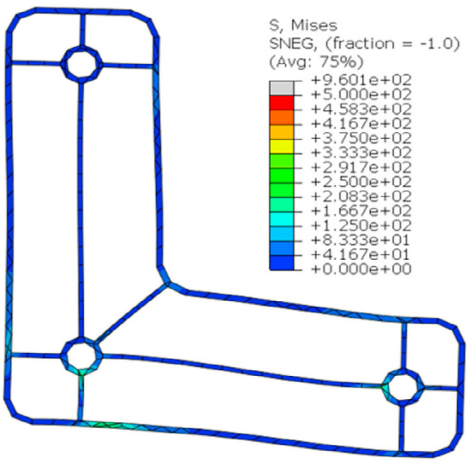

Fig. 13. Von Mises Stress at a force of 200N

Fig. 14. Top view of the printed object along with its corresponding support structure

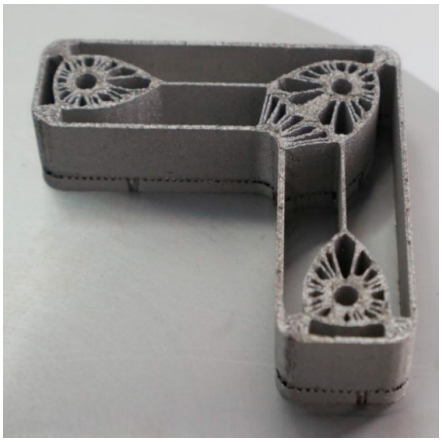

Fig. 15. A perspective view of the knot and the printed support structure

It would surely be interesting to explore this possibility in future work. Finally, the metal knots should be simulated for several rip structures and rip thicknesses and the performance will be evaluated in experimental load tests. Even the relaxation behavior should be investigated.

References

[1] Stava O, Vanek J, Benes B, Carr N, Měch R. Stress relief: Improving structural strength of 3D printable objects. ACM Trans Graph 2012; 31(4): 48:1-48:11.

[2] Zhou Q, Panetta J, Zorin D. Worst-case structural analysis. ACM Trans Graph 2013; 32(4): 137:1-137:12.

[3] Prévost R, Whiting E, Lefebvre S, Sorkine-Hornung O. Make it stand: Balancing shapes for 3D fabrication. ACM Trans Graph 2013; 32(4): 81:1-81:10.

[4] Bächer M, Whiting E, Bickel B, Sorkine-Hornung O. Spin-it: Optimizing moment of inertia for spinnable objects. ACM Trans Graph 2014; 33(4): 96:1-96:10.

[5] Bickel B, Bächer M, Otaduy MA., Lee HR, Pfister H, Gross M, Matusik W. Design and fabrication of materials with desired deformation behavior. ACM Trans Graph 2010; 29(4): 63:1-63:10.

[6] Blum H. A transformation for extracting new descriptors of shape. In: Wathen-Dunn W, editors. Models for the Perception of Speech and Visual Form. Cambridge: MIT Press; 1967. p. 362-380.

[7] Siddiqi K, Pizer S, editors. Medial Representations: Mathematics, Algorithms and Applications. Netherland Springer; 2008.

[8] Breuß M, Bruckstein AM, Maragos P, editors. Innovations for Shape Analysis, Models and Algorithms. Berlin (Germany): Springer; 2013.

[9] Xu W, Li W, Liu L. Skeleton-Sectional Structural Analysis for 3D Printing. J Comput Sci Technol 2016; 31:439–49.

[10] Ding D, Pan Z, Cuiuri D, Li H. A practical path planning methodology for wire and arc additive manufacturing of thin-walled structures. Robot Comput Integr Manuf. 2015; 3:8-19.

[11] Kao JH, Prinz FB. Optimal motion planning for deposition in layered manufacturing. In: Proc ASME Des Eng Tech Conf; 1998.

[12] Siddiqi K, Bouix S, Tannenbaum A, Zucker SW. Hamilton-Jacobi skeletons. Int J Comput Vision 2002; 48, 215-31.

[13] Peter P, Breuß M. Refined Homotopic Thinning Algorithms and Quality Measures for Skeletonisation Methods. In: Breuß M, Bruckstein AM, Maragos P, editors. Innovations for Shape Analysis. Berlin (Germany): Springer; 2013. p. 77-92.

[14] Maurer CR, Qi R, Raghavan V. A Linear Time Algorithm for Computing Exact Euclidean Distance Transforms of Binary Images in Arbitrary Dimensions. IEEE Trans Pattern Anal Mach Intell. 2003; 25:256-70.

[15] Pudney C. Distance-Ordered Homotopic Thinning: A Skeletonization Algorithm for 3D Digital Images. Comput Vis Image Underst. 1998; 72(3):404–13.

[16] Soille P. Morphological Image Analysis. Berlin (Germany): Springer; 2004.

[17] Buhl J, Israr R, Bambach M. Modeling and convergence analysis of directed energy deposition simulations with hybrid implicit/explicit and implicit solutions. Journal of Machine Engineering. 2019; 19(3):94-107.